

Study of Photodissociation Dynamics Using Sub-Doppler Fluorescence Imaging Method: Photodissociation of ICN at 308 nm

Jia-lin Chang^{a*} (張嘉麟), Kuo-mei Chen^b (陳國美),
Wei-yu Lin^b (林維昱) and Yit-Tsong Chen^{a,c*} (陳逸聰)

^a*Institute of Atomic and Molecular Sciences, Academia Sinica, P.O. Box 23-166,
Taipei 106, Taiwan, R.O.C.*

^b*Department of Chemistry, National Sun Yat-sen University, Kaohsiung, Taiwan, R.O.C.*

^c*Department of Chemistry, National Taiwan University, Taipei 106, Taiwan, R.O.C.*

The sub-Doppler fluorescence imaging method has been developed to determine velocity distribution, angular distribution, and vector correlation of state-selected photofragments. Using this new method, photodissociation dynamics can be studied directly in the center-of-mass frame, even with an uncollimated molecular beam. We have performed the experiment of photodissociation of ICN at 308 nm to demonstrate that recoil velocities of photofragments can be obtained without collimating the parent beam. The forward- and backward-scattered CN($X^2\Sigma^+$) photofragments are imaged simultaneously for the first time. The recoil velocities of the CN photofragments are measured and the bond dissociation energy $D_0^0(\text{I-CN})$ is determined to be $26960 \pm 120 \text{ cm}^{-1}$, in agreement with the literature values reported recently.

1. INTRODUCTION

Recently, we have proposed and developed a "sub-Doppler fluorescence imaging method" (SFIM) to determine velocity distribution, angular distribution, and vector correlation of photofragments in the studies of photodissociation dynamics.¹ This method modifies the fluorescence imaging techniques which were first applied by Chen et al. to investigate photodissociation and reaction dynamics.²⁻⁸ To obtain better velocity and angular resolutions using conventional fluorescence imaging techniques, the reaction zone has to be confined in a tiny volume, which can be achieved by crossing a well-collimated molecular beam with another well-collimated reagent beam or a focused laser beam. The drastic decrease in the number density of reaction products due to the expansion following the event of bimolecular collisions or photodissociation, unfortunately, has limited the number of fluorescence imaging experiments.⁴⁻⁶ Nevertheless, it has been shown in our theoretical study of SFIM that three-dimensional (3D) dynamics of state-selected photofragments can be measured directly in the center-of-mass frame (CMF), even with an uncollimated molecular beam.¹ By doing such, the signal-to-noise ratio should be progressively improved because a larger number density of parent molecules can be retained. The relevant theories of SFIM have been derived using density matrix formalism. The feasibility of this new method has also been demonstrated by the experiment of la-

ser ablation of B atoms at 248 nm.¹

In this paper, we report the photodissociation experiment of cyanogen iodide (ICN) at 308 nm to demonstrate that recoil velocities of state-selected photofragments can be measured in an uncollimated molecular beam, as the original proposal claimed.¹ The forward- and backward-scattered CN photofragments are imaged simultaneously for the first time, from which the bond dissociation energy $D_0^0(\text{I-CN})$ is determined.

The rest of this paper is organized as follows. Section 2 gives an overview for the design of SFIM. Next, Section 3 describes the details of the ICN photodissociation experiment, and Section 4 presents and discusses the results. Finally, conclusions are addressed in Section 5.

2. OVERVIEW OF SFIM

Fig. 1a shows the experimental design of SFIM for the studies of photodissociation dynamics using a linearly polarized photodissociation laser. The time sequences for every experimental event are displayed in Fig. 1b. In general, the target molecular beam is expanded into the vacuum by a pulsed valve. A photodissociation laser crosses the molecular beam in the collisionless regions. Then a laser sheet, counter-propagating with the photodissociation laser, probes the photofragments distributed in the plane defined by the molec-



ular and photodissociation laser beams at a selected delay time with respect to the onset of photodissociation. The bandwidth of the probe laser should be much less than the Doppler widths of the photofragments for the purpose of selecting certain velocities of photofragments along the propagating direction of the probe laser. The internal state distribution of the photofragments is determined by the probe laser via a laser-induced fluorescence (LIF) technique. A 2D imaging detector, e.g., an intensified charge-coupled device (CCD) camera, is utilized to register the spatial positions of the photofragments by detecting the emitted fluorescence. The polarization-states of the emitted fluorescence can be analyzed by mounting a linear polarizer in front of the CCD camera.

Assume that the probe laser propagates along the Y-direction and the CCD detector is mounted in the X-direction (Fig. 2), then the direct extraction of 3D distribution of the photofragments is accomplished by the following procedures. (1) The thin laser sheet slices the YZ-plane of the expanded Newton sphere and selects the photofragments with the velocity component $v_x = 0$ (Fig. 2a). (2) The sub-Doppler

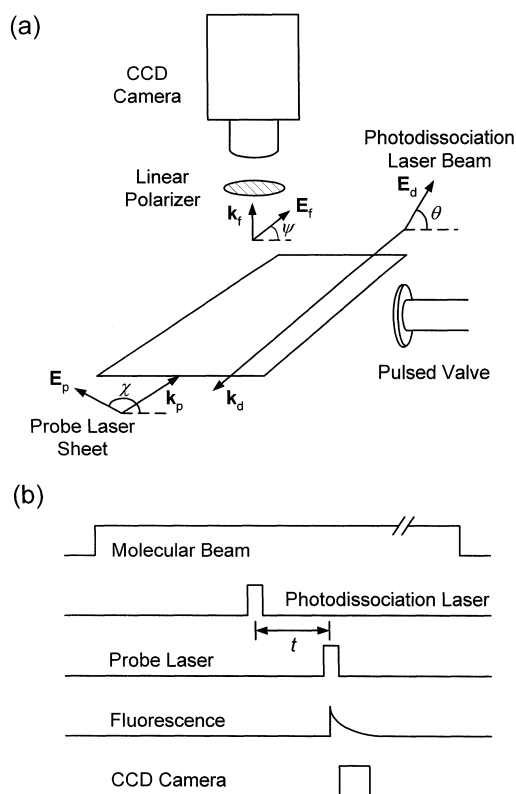


Fig. 1. (a) Schematic diagram of the experimental setup for the sub-Doppler fluorescence imaging method. (b) The time sequences for every experimental event (not to scale).

laser frequency selects the photofragments with $v_y = c(\nu - \nu_0)/\nu$ (Fig. 2b), where ν is the laser frequency, ν_0 is the Doppler-free molecular transition frequency, and c is the speed of light. (3) Finally, the distribution of photofragments in the Z-dimension is determined from fluorescence image using $v_z = Z/t$ (Fig. 2c), where Z is the distance measured from the CM of photofragments, and t is the delay time between the probe and photodissociation lasers with short pulse duration (< 20 ns). Due to the Doppler velocity selection in the Y-direction, the parent molecular beam need not be well collimated. For parallel beams with multiple photolysis centers, the image of photofragments is like that depicted in Fig. 2c; for beams moving with a slight curvature, the image is shown in Fig. 2d. It can be realized from Fig. 2c that the image patterns along the Z-dimension are the same for every photolysis center of different initial Y-positions. Therefore, the signals in the Y-dimension can be integrated over to improve the signal-to-noise ratio, and only the image profiles along the Z-dimension are necessary for determining the velocity and angular distribution of photofragments.

Two schemes of SFIM have been proposed.¹ Design of Scheme I fixes the polarization vector (E_d) of the photodissociation laser at $\theta = 0^\circ$ (Fig. 1) and scans the frequency of the probe laser. For each frequency, i.e., for each selected v_y , the v_z -components of photofragments are determined from the recorded image. After scanning ν to cover the whole Doppler profile of photofragments, velocity and angular distributions of photofragments in a specific quantum-state can

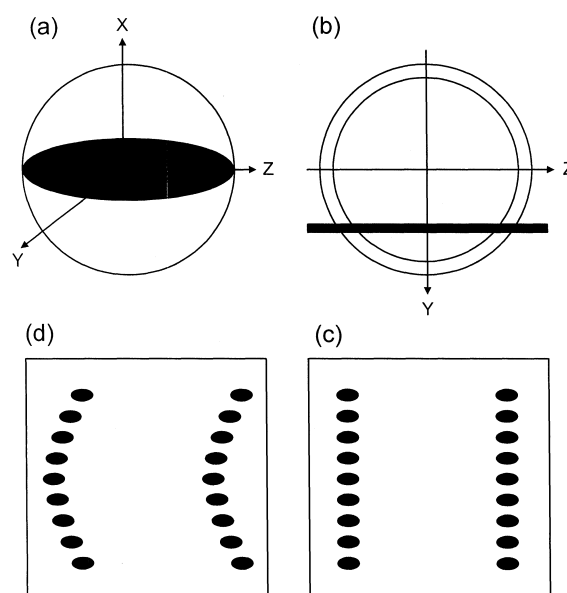


Fig. 2. Schematic diagram for direct extraction of the 3D distribution of photofragments (see text).

be analyzed from $I_{exp}(v_x=0, v_y, v_z)$, where I_{exp} is the measured fluorescence intensity as a function of velocities in the YZ-plane. On the other hand, Scheme II measures the fluorescence intensity $I_{exp}(v, \theta)$ as a function of velocity and scattering angle, i.e., the frequency of the probe laser is fixed at ν_0 to single out the photofragments with $v_y = 0$, and E_d is varied (Fig. 1). At each selected θ , the velocities along this scattering angle are determined from the image. Scheme II is more versatile than Scheme I when using a linearly polarized photodissociation laser,¹ but Scheme I is more general and can be applied for other experiments of molecular dynamics. For example, Scheme I has been successfully applied to study the laser ablation mechanisms of B atoms at 248 nm, which clearly demonstrates the feasibility of SFIM.¹

The relevant theories of SFIM have been derived for Scheme I and Scheme II using density matrix formalism by Chen and Chang⁷ and Chang et al.,¹ respectively. For instance, the fluorescence intensity formula of Scheme II can be written as¹

$$I_{exp} = CP(v)P(\theta)I_p(J_1, J_2, J_3, v, \theta, \chi, \psi) \quad (1)$$

where C is a proportion constant, $P(v)$ is the velocity distribution function, $P(\theta)$ is the angular distribution function, and

$$I_p(J_1, J_2, J_3, v, \theta, \chi, \psi) = S_1 S_2 \sum_{k,q} X_q^k(J_1, J_2, J_3, \chi, \psi) \rho_q^k(J_1, v, \theta) \quad (2)$$

where S_i is the transition amplitude, J_i is the rotational quantum number, ρ_q^k is the state multipole of rank k with component q , and X_q^k is the corresponding coefficient of ρ_q^k .¹ The effects of anisotropic distributions of the photofragment rotational angular momenta on the fluorescence intensities are embedded in I_p . Explicit forms of the above equations can be found in Refs. 1 and 7.

Without a priori knowledge for the photodissociation system of interest, the polarization effects of the photofragment rotational angular momenta on the fluorescence intensities should always be clarified before one can extract the velocity and angular distributions of photofragments from the LIF detection scheme. That is, I_p in eq 2 ought to be determined prior to the measurements of $P(v)$ and $P(\theta)$. In a 1+1 LIF detection scheme, eight alignment parameters (i.e., ρ_{0-2}^2 and ρ_{0-4}^4) can be uniquely determined by varying the χ - and ψ -angles through two types of transitions (e.g., P and Q or R and Q), for a minimum number of 13 measurements.¹ When the eight parameters are known for the photofragments with

selected v and θ , $P(\theta)$ can be determined by varying θ , and $P(v)$ can be obtained at the magic angle (i.e., $\theta = 54.73^\circ$) where $P(\theta)$ becomes a constant for all v .¹

3. EXPERIMENTAL SECTION

In order to illustrate that recoil velocities of photofragments can be obtained with an uncollimated molecular beam, we have performed a photodissociation experiment of ICN at 308 nm. In the photodissociation of ICN at this wavelength, Fisher et al. measured the internal energy distributions of the CN photofragments using LIF spectroscopy,⁹ and Hall and co-workers studied vector correlations of photofragments using high-resolution transient frequency modulated absorption spectroscopy.^{10,11} The experimental setup for the photodissociation of ICN at 308 nm was similar to that depicted in Fig. 1 except that no polarization studies were made. The experimental procedures have already been described in Sec. 2. Specifically, a neat beam of ICN (~ 110 Torr) was expanded into vacuum ($\sim 10^{-6}$ Torr) by a pulsed valve (General Valve, Series 9) with an orifice of 0.8 mm in diameter. The nozzle was kept at 100 °C during the experiment. The pulse duration of the parent beam was $\sim 800 \mu\text{s}$, and the pressure of the vacuum system increased to $\sim 5 \times 10^{-5}$ Torr when the pulsed valve was operated at 3 Hz.

The photodissociation laser was the output of a XeCl excimer laser (Lambda Physik, Compex 200) and was aligned to cross the ICN beam ~ 12 mm downstream the nozzle. Note that when the photodissociation laser was positioned at shorter distances (< 6 mm) relative to the nozzle, quite different image patterns were obtained showing that the CN photofragments collided with the remaining ICN molecules. The probe laser was the output of a dye laser (Lambda Physik, LPD 3000) pumped by another XeCl excimer laser (Lambda Physik, LPX 200). The CN photofragments were detected via LIF of the transition $\text{CN}(B^2\Sigma^+, v=0) \leftarrow \text{CN}(X^2\Sigma^+, v=0)$. The 2D imaging detector was an ICCD (Princeton Instruments, 576G/RB) with an electronic shutter gated at a pulse of 100 ns. The time sequence for each instrument was controlled by a digital pulse/delay generator (Stanford Research, DG535).

4. RESULTS AND DISCUSSION

Fig. 3 depicts the excitation spectrum of the nascent CN photofragments generated from the photodissociation of ICN



at 308 nm in a flow ing cell con tain ing 15 mTorr ICN. The CN spec trum ob tained in this work is con sis tent with that re ported by Fisher et al.⁹ While the P-branch peaks of the CN spec trum are clus tered to gether for the $B \leftarrow X$ tran si tions, the R-branch peaks are well sep a rated from each other (Fig. 3). A strong band-head is formed around 388.34 nm for the P-branch owing to $B' = 1.9701 \text{ cm}^{-1} > B'' = 1.8996 \text{ cm}^{-1}$.¹² The weak sig nals present in the vi cin ity of the $v'' = 0$ peaks are due to the $\text{CN}(B^2\Sigma^+, v' = 1) \leftarrow \text{CN}(X^2\Sigma^+, v'' = 1)$ tran si tions. The im ages of the CN photofrag ments were taken at the res onance fre quen cies for the se lected quan tum-states.

Figs. 4a-4c show three im ages of CN probed at the de lay times of 0.2, 1.1 and 2.1 μs , re spec tively, af ter the photo-

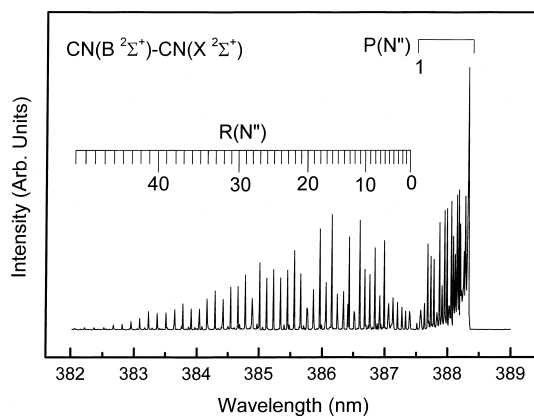


Fig. 3. Ex ci ta tion spec trum of the $\text{CN}(X^2\Sigma^+)$ photofrag ments gen er ated from the photo dis so ci a tion of ICN at 308 nm.

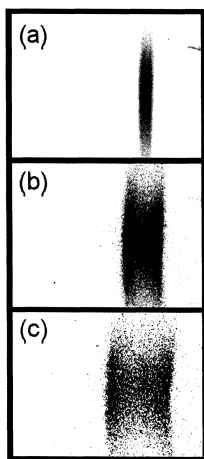


Fig. 4. Im ages of $\text{CN}(X^2\Sigma^+)$ photofrag ments probed at 388.34 nm with a de lay time of (a) 0.2, (b) 1.1, and (c) 2.1 μs af ter photo dis so ci a tion of ICN at 308 nm.

dis so ci a tion of ICN at 308 nm. The im ages in Fig. 4a-4c were ob tained by av er ag ing 5, 600, and 1800 la ser shots, re spec tively. The probe la ser was tuned at the band-head of the P-branch (388.34 nm) to de tect the $\text{CN}(X^2\Sigma^+, v'' = 0, N'' = 27-30)$ photofrag ments.¹² Sim i lar im ages with poorer sig nal-to-noise ra tios (not shown) were also ob tained for the CN frag ments in a sin gle ($v'' = 0, N''$) rovibra tional state by the LIF of CN through the R-branch. As men tioned ear lier in Sec. 2, the cur va ture in the ver ti cal di rec tion of Fig. 4 is due to un col li mated par ent beams (cf. Fig. 2d), and only the im age pro file along hor i zon tal di rec tion is use ful in the ve loc ity de ter mi na tion. The im age pro files of Figs. 4a and 4c are dis played in Figs. 5a and 5b, re spec tively. The fol low ing con clu sions can be de duced di rectly from Figs. 4 and 5. (1) The for ward- and back ward-scattered photofrag ments are im aged si mul ta neously. Ac cord ingly, the av er age re coil ve loc ity of the CN photofrag ments can be de ter mined to be $1800 \pm 25 \text{ m/s}$, cal cu lated di rectly from Fig. 5b where the dis tance be tween the for ward and back ward peaks is marked. Due to the con ser va tion of (linear) mo men tum, the av er age re coil ve loc ity of the coun ter part I atomic photofrag ments is $369 \pm 6 \text{ m/s}$. (2) The im age pro files are sym met ric and sin gle-peaked in both the for ward and back ward di rec tions (Fig. 5b) mean ing that only one photo dis so ci a tion chan nel is ac tive, i.e., $\text{ICN} + h\nu(308 \text{ nm}) \rightarrow \text{I}(^2\text{P}_{3/2}) + \text{CN}(X^2\Sigma^+)$. The $\text{I}^*(^2\text{P}_{1/2})$ at oms were not pro duced in the photo dis so ci a tion of ICN at 308 nm. The bond dis so ci a tion en ergy $D_0^0(\text{I-CN})$ can be cal cu lated by

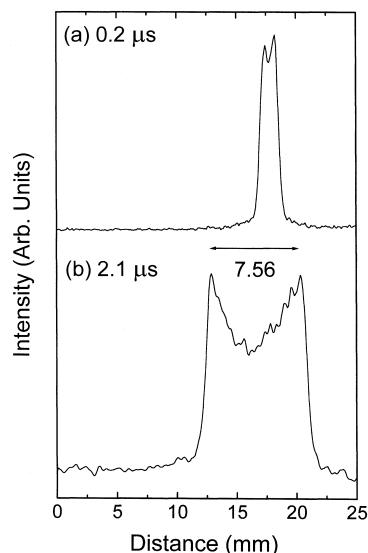


Fig. 5. Im age pro files of CN taken from (a) Fig. 4a and (b) Fig. 4c. The ar rows de note the dis tance be tween the for ward and back ward peaks.

$$D_0^0(\text{I-CN}) = h\nu + E_i(\text{ICN}) - E_i(\text{CN}) - \frac{1}{2}m_{\text{CN}}v_{\text{CN}}^2 - \frac{1}{2}m_1v_1^2 \quad (3)$$

where $h\nu = 32647 \text{ cm}^{-1}$ is the energy of a photon at 308 nm, $E_i(\text{ICN}) = 340 \text{ cm}^{-1}$ is the internal energy of the parent ICN molecules (see a later discussion), $E_i(\text{CN}) = 1600 \text{ cm}^{-1}$ is the average internal (rotational) energy of the detected CN photofragments (Fig. 4), and the last two terms are the kinetic energies of photofragments. By inserting all the above values into eq 3 and considering the uncertainty in the measurement of the CN velocities, one has $D_0^0(\text{I-CN}) = 26960 \pm 120 \text{ cm}^{-1}$. (3) Finally, the parent ICN beams move at an average velocity of $610 \pm 25 \text{ m/s}$ in the laboratory frame, determined from the movement of the CM of the CN photofragments (Figs. 4 & 5). This is due to the fact that the CM velocity of photofragments is identical to that of the parent molecules, since no external forces are imposed on the photodissociation system. Consequently, once the images of photofragments are obtained, like those in Fig. 4, the analysis of photodissociation dynamics is quite simple and straightforward.

In this work, the bandwidth ($\sim 0.2 \text{ cm}^{-1}$) of the probe laser was only slightly less than the width ($\sim 0.3 \text{ cm}^{-1}$) between the maximum and minimum Doppler shift of the CN photofragments. In addition to the effects of recoil velocities, the image profiles in Fig. 5 are therefore blurred by the photofragments scattered at any angle within the probing area of the laser sheet, the velocity spreads of the parent beams, and the contribution from different quantum states. However, the images in Fig. 4 clearly demonstrate that the forward- and backward-scattered photofragments can be simultaneously detected by the fluorescence imaging techniques. Hence, when the bandwidth of the probe laser is improved to be sub-Doppler for a single state of photofragments, the image profiles will show two distinct and well-resolved peaks, which result from the recoil velocities of photofragments with minor contributions from velocity spreads of the jet-cooled parent beams. Following the experimental procedures proposed by Chang et al.,¹ velocity distribution, angular distribution, and vector correlation of state-selected photofragments can be determined accordingly.

Note that the internal energy $E_i(\text{ICN})$ was not characterized in this work and was taken as 340 cm^{-1} , assuming that the CN photofragments are generated predominantly from ICN in its first vibrational state (bend, 304 cm^{-1})¹³ with rotational temperature $\sim 50 \text{ K}$, estimated from the measurement of rotational temperature for NO_2 molecular beams. It is believed

that vibrational hot bands play an important role in the red wing of the ICN absorption spectra in the \tilde{A} band continuum, such as at 308 nm.⁹⁻¹¹ We support this argument by the finding that the CN fluorescence intensities were reduced as the ICN molecules were seeded in 1 atm He serving as carrier gas. We therefore assume that the vibrationally excited states are responsible for the photodissociation of ICN at 308 nm. Without the assumption for the internal energy of the ICN molecules, a lower bound for $D_0^0(\text{I-CN}) = 26620 \pm 120 \text{ cm}^{-1}$ can be determined by setting $E_i(\text{ICN}) = 0$ in eq 3. The value of $D_0^0(\text{I-CN}) = 26960 \pm 120 \text{ cm}^{-1}$ determined in this work is in agreement with the literature values reported recently, such as $26980 \pm 100 \text{ cm}^{-1}$ by Hall and co-workers¹¹ and $26500 \pm 500 \text{ cm}^{-1}$ by Wittig and co-workers.¹⁴ In a preliminary fluorescence imaging experiment of photodissociation of ICN at 248 nm,⁴ however, the $D_0^0(\text{I-CN})$ was determined to be $28700 \pm 100 \text{ cm}^{-1}$. This value was probably overestimated because, in that work, only the forward-scattered CN photofragments were detected and the CM velocity of the parent beam was not measured. In contrast, simultaneous detection of the forward- and backward-scattered photofragments (Fig. 4) allows us to unambiguously determine the recoil velocities of photofragments directly in the CMF. As such, the CM velocity of the parent beam need not be measured, albeit it can be inferred from the images of photofragments, as already shown above.

At this point, we shall compare fluorescence imaging with the well-developed ion imaging technique.^{15,16} While fluorescence imaging adopts LIF techniques to probe reaction products, ion imaging detects products via resonance-enhanced multiphoton ionization (REMPI). It is generally accepted that a REMPI technique is more sensitive than LIF. In an ion imaging experiment, however, only a very few ions can be generated per laser shot; otherwise space charge effects can seriously destroy the velocity distribution of the nascent products. To obtain an ion image with reasonable quality, the signals have to be averaged for $\sim 10^4$ laser shots. In sharp contrast, fluorescence imaging detects photons emitted from neutral molecules; the number density of products can therefore be controlled as high as possible under collision-free conditions. It takes $\sim 10^3$ laser shots to accumulate a good fluorescence image (e.g., Fig. 4c). Besides, both imaging techniques are able to determine not only velocity and angular distributions, but also vector correlations of state-resolved products. The usage of either technique will depend on whether the target molecules are suitable for the LIF or REMPI detection schemes.



5. CONCLUSIONS

The new "sub-Doppler fluorescence imaging method" has been shown to be a useful tool in the studies of photodissociation dynamics. The photodissociation of ICN at 308 nm demonstrates that recoil velocities of state-selected photofragments can be measured with an uncollimated molecular beam. The forward- and backward-scattered CN($X^2\Sigma^+$) photofragments are imaged simultaneously for the first time. The bond dissociation energy $D_0^0(\text{I-CN})$ is determined to be $26960 \pm 120 \text{ cm}^{-1}$, in agreement with the literature values reported recently.

The preliminary results shown in this paper promise detailed investigations of photodissociation dynamics using this technique. It is most valuable if polarization experiments can be performed. By varying the vectors of the linearly polarized photolysis and probe lasers, anisotropy parameters and vector correlations can be measured for the state- and velocity-selected photofragments.¹ The experiment of ICN photodissociation including polarization studies is underway.

ACKNOWLEDGEMENTS

This work is supported by the National Science Council of the ROC. J.L.C. is grateful to Academia Sinica for his postdoctoral fellowship at IAMS.

Received December 31, 2000.

Key Words

Sub-Doppler; Fluorescence imaging;

Photodissociation; Cyanogen iodide.

REFERENCES

1. Chang, J.; Chen, K.; Lin, W.; Lee, K.; Chen, Y.-T. *J. Chem. Phys.* **2000**, *113*, 5716.
2. Chen, K. *Chem. Phys. Lett.* **1992**, *198*, 288.
3. Chen, K.; Pei, C. *Chem. Phys. Lett.* **1994**, *217*, 471.
4. Chen, K.; Kuo, C.; Tzeng, M.; Shian, M.; Chung, S. E. *Chem. Phys. Lett.* **1994**, *221*, 341.
5. Chen, K.; Sung, C.; Chang, J.; Chung, T.; Lee, K. *Chem. Phys. Lett.* **1995**, *240*, 17.
6. Chen, K.; Lee, K.; Chang, J.; Sung, C.; Chung, T.; Liu, T.; Perng, H. *J. Phys. Chem.* **1996**, *100*, 488.
7. Chen, K.; Chang, J. *J. Phys. Chem. A* **1997**, *101*, 2525.
8. Chen, K.; Pei, C. *J. Chem. Phys.* **1998**, *109*, 6647.
9. Fisher, W. H.; Carington, T.; Filseth, S. V.; Sadowski, C. M.; Dugan, C. H. *Chem. Phys.* **1983**, *82*, 443.
10. North, S. W.; Mueller, J.; Hall, G. E. *Chem. Phys. Lett.* **1997**, *276*, 103.
11. Costen, M. L.; North, S. W.; Hall, G. E. *J. Chem. Phys.* **1999**, *111*, 6735.
12. Herzberg, G. *Molecular Spectroscopy and Molecular Structure I. Spectra of Diatomic Molecules*; Van Nostrand Reinhold: New York, 1950.
13. Thompson, G.; Maki, A. G. *J. Mol. Spectrosc.* **1993**, *160*, 73.
14. Nadler, I.; Mahgerefteh, D.; Reisler, H.; Wittig, C. *J. Chem. Phys.* **1985**, *82*, 3885.
15. Chandler, D. W.; Houston, P. L. *J. Chem. Phys.* **1987**, *87*, 1445.
16. Heck, A. J.; Chandler, D. W. *Annu. Rev. Phys. Chem.* **1995**, *46*, 335.

